Supplementary Materials II

Computational Fluid Dynamics Simulation (CFD)

Two-dimensional, incompressible laminar flow with chemical reactions was modeled within the geometry shown in Figure 1a using Fluent™ v13.0, a finite-volume CFD component in ANSYS Workbench™ (Ansys, Inc). The simulation of the flow profile in a top microchannel of a 3D μCA (microfluidic cell array) was modeled by incompressible form of Navier-Stokes equation.

$$\rho\left(\frac{\partial \mathbf{u}}{\partial t}+\mathbf{u}\cdot\nabla\mathbf{u}\right)=-\nabla p+\mu\nabla^2\mathbf{u} \tag{1}$$

where variables are defined as μ for kinematic viscosity, **u** for fluid particle speed, ρ for fluid density and p for fluid pressure at a point in the fluid. Hydrogel with cells in a bottom microchamber of a μCA was modeled as a porous medium and the flow profile there was numerically solved based on Darcy's law.

The reaction rate and concentration of constituent species depend on each other, and they are ultimately governed by advective and diffusive transport mechanisms driven by the fluid flow. For modeling species transport, the conservation equation was used, which takes the general form of

$$\frac{\partial}{\partial t}(\rho m)+\frac{\partial}{\partial x}(\rho u m)=-\frac{\partial}{\partial x}J+R+S \tag{2}$$

where m is the mass fraction, J is the diffusion flux of species, R is the mass rate of creation or depletion by chemical reaction and S is the rate of creation by addition from the dispersed phase. In our model, there was no term of "*S*".

For solving Eqn. (1), Fluent was set to invoke pressure-based algorithm based on SIMPLE scheme for pressure-velocity coupling. Spatial and transient discretizations were set to be of second-order for all sets of governing equations. A steady-state solution was obtained after letting the solver run for a sufficiently large simulation time and converge to equilibrium state. The boundary condition at the inlet was uniform flow of the nutrient solution at 37 °C with 100 μm/s speed. The saturation concentration of O_2 dissolved from air at 1 atm is about $[O_2]=6.9\times10^{-6}$ g/g [1] . This concentration value was supplied as the inlet boundary condition for the mass fraction of O_2. The mass fraction of glucose at the inlet was given as $[C_6H_{12}O_6]=1\times10^{-3}$ g/g, which is a value close to the after-meal blood sugar level of healthy humans [2]. The outlet boundary condition was set to zero gage pressure. The rest of the solid boundaries are specified as impermeable walls where the no-slip condition on the fluid velocity was imposed. The hydrogel-filled chamber was modeled as a saturated porous zone with 99% porosity in accordance with the water volume fraction provided by its manufacturer. The permeability[3] of collagen I at 2mg/ml is $2\times10^{-12}m^2$. Considering the stiffness of 0.25% Puramatrix is close to 2mg/ml Collagen I [4] , $2\times10^{-12}m^2$ was used in our CFD simulation. The reciprocal of this value was supplied to the solver as the viscous resistance coefficient. The widths of the ten openings in the membrane model were determined such that the actual membrane and its two-dimensional model have the same solidity (i.e. the ratio of open area to the total area of the membrane). Since PDMS is gas-permeable, the membrane should allow diffusion of O_2 and CO_2 while blocking diffusion of glucose through its body, permitting glucose advection only through the openings of the membrane. In order to simulate this behavior, the membrane was modeled as another water-saturated porous medium with very small permeability ($K_1=2\times10^{-16}$ m^2) to inhibit advection inside the membrane body. The diffusion coefficients in the solution were set as $D_{CO_2}=16\times10^{-10}$

m^2/s [5], $D_{O_2}=21x10^{-10}$ m^2/s [6], and $D_{C_6H_{12}O_2}=7x10^{-10}$ m^2/s [7]. Due to the lack of literature data for diffusion coefficients of the species at 37 °C in PDMS, the same diffusion coefficients inside the membrane were used for oxygen and carbon dioxide except glucose. The diffusion of glucose inside the membrane was inhibited by setting its coefficient to a very small value, i.e. $D_{C_6H_{12}O_2}=1x10^{-20}$ m^2/s.

While it is known that aerobic respiration is a complex reaction of multiple steps, the chemical reaction model in this study simply considered the total reaction of aerobic respiration [8]

$$C_6H_{12}O_6 + 6O_2 \rightarrow 6CO_2 + 6H_2O \quad (3)$$

The rate of this reaction not only depends on the temperature and the concentrations of the reactants and the products but also on the enzymatic activity involved in the sub-reactions. Assuming an abundant glucose supply, the reaction is rate-limited by temperature, and O_2 and CO_2 concentrations, as modeled by a Michaelis-Menten type of equation in terms of O_2 consumption [9]:

$$r_{O_2} = \frac{v_m [O_2]}{k_m + \left(1 + \frac{[CO_2]}{k_i}\right)[O_2]} \quad (4)$$

where $[O_2]$ and $[CO_2]$ are concentrations of oxygen and carbon dioxide expressed in mass fractions, v_m is the maximum respiration rate, k_m is Michaelis-Menten constant and k_i is non-competitive inhibition constant. Several experimental studies for determining the reaction rates, constants and their dependencies on temperature for post-harvest respiration of various fresh produce were presented in the literature [9-13].

The dependency of the reaction rate to temperature was found by fitting the variation of reaction parameters in Arrhenius type of an equation

$$A = A_0 \exp\left(\frac{-E_a}{RT}\right) \tag{5}$$

where A was a temperature-dependent reaction parameter (v_m, k_m or k_i), A_0 was a pre-exponential factor, R=8.314 kJ kg^{-1} K^{-1} was the universal gas constant, T is the absolute temperature in Kelvins and E_a was "activation energy" for fitting the parameter in variations of T. The experimental data presented in [9] provides the following A_0 and E_a values for the respiration of apples:

for v_m: A_0=4.3x10^6 ml kg^{-1} h^{-1} and E_a=29150 kJ kg^{-1} mol^{-1} (6a)

for k_m: A_0=1.3x10^4 and E_a=18030 kJ kg^{-1} mol^{-1} (6b)

for k_i: A_0=1.8x10^{-3} and E_a=-20290 kJ kg^{-1} mol^{-1} (6c)

When used in Eqn.s (6) and (5), these values yield the reaction rate in "ml of O_2 consumption in an hour per kg of apples", with units of ml kg^{-1} h^{-1}. However, Fluent requires the input to be given in [kmol m^{-3} s^{-1}] for consumption of the species with a stoichiometric coefficient of unity, which is glucose for the reaction shown in Eqn. (3). The rate of the reaction in required units was then found as

$$r_{C_6H_{12}O_6}\left[\text{kmol m}^{-3}\text{s}^{-1}\right] = r_{O_2}\left[\text{ml kg}^{-1}\ \text{h}^{-1}\right]\frac{M_a[\text{kg}]}{V[\text{ml}]}\frac{\rho[\text{kg m}^{-3}]}{m_{O_2}[\text{kg kmol}^{-1}]}\frac{1}{60[\text{s min}^{-1}]60[\text{min h}^{-1}]}\frac{1}{6} \tag{7}$$

where M_a=1.3108 kg is the mass of apples, V=4101.98x10^{-6} m^3 is the volume occupied by oxygen in the container, ρ=993.33 kg/m^3 is the density of the solution in our simulation, $m_{O_2} = 64$ kg/kmol is the mass per kilomol of oxygen, and 6 is the stoichiometric coefficient of oxygen in Eqn. (3). Note that the apple mass per container volume used in the work by Mahajan

[9] is about M_a/V=320 kg/m^3. With an average density of 1100 kg/m^3 [3, 14] and diameter of 15 μm, the mass of 5000 spherical cells per the chamber volume was found to be about 239 kg/m^3, which justifies the usage of data from the large-scale experiment presented in[9] in this small-scale simulation.

The rate expression shown in Eqn. (4) was implemented in *Fluent* solver by means of a user defined function (UDF) script external to the software. In the script, the rate of oxygen generation was first calculated using equations (4) to (6) based on the local values of temperature and mass fractions of oxygen and carbon dioxide in the chamber. The rate was then converted in appropriate units using Eqn. (7). Finally, the rates of production and destruction of the species were obtained by multiplying the value of $r_{C_6H_{12}O_6}$ by their respective stoichiometric coefficients in Eqn. (3). In this model, it is assumed that cells are homogenously distributed within the hydrogel, therefore the reaction mechanism is introduced into *Fluent* as a volumetric reaction taking place in the chamber.

RESULTS

Diffusion and microcirculation profile using computational fluid dynamics (CFD) analysis

The steady state result of the computational simulation on flow and reaction dynamics in the device is shown in Figure 1b to 1d. The maximum velocity in a top microchannel is about150 μm/s at the channel center (Fig. 1b). A close look inside a bottom microchamber reveals an extremely low advective flow at about 0.1 μm/s (Fig. 1b), which is similar to an interstitial flow rate in vivo [3, 15]. The contours of O_2 (oxygen) and CO_2 (carbon dioxide) concentrations are shown in Figure 1c. The decrease in O_2 concentrations from the microchannel inlet to bottom right corner of a microchamber respectively is less than 0.0003%. Figure 1c also shows that

very small amount of CO_2 ($4x10^{-11}$ g/g) from metabolic reactions do accumulate at the downstream of a microchamber. However, $4x10^{-11}$ g/g of CO_2 in microchambers is negligible comparing to normal CO_2 concentration in cell culture media, which is 4.709 x 10^{-5} g/g calculated by application of Henry's Law using a CO_2 solubility of 0.03 mM/mmHg and CO_2 partial pressure of 712 mmHg*5% or 35.6mmHg. Figure 1d illustrates a uniform glucose distribution in microchannels and microchambers when the resolution of the scale is set to 0-0.001 g/g. Simulation data conclude that vertical diffusion between different layers plus convection flow in the top microchannels is sufficient for nutrient delivery and waste removal in the 3D μFCA.

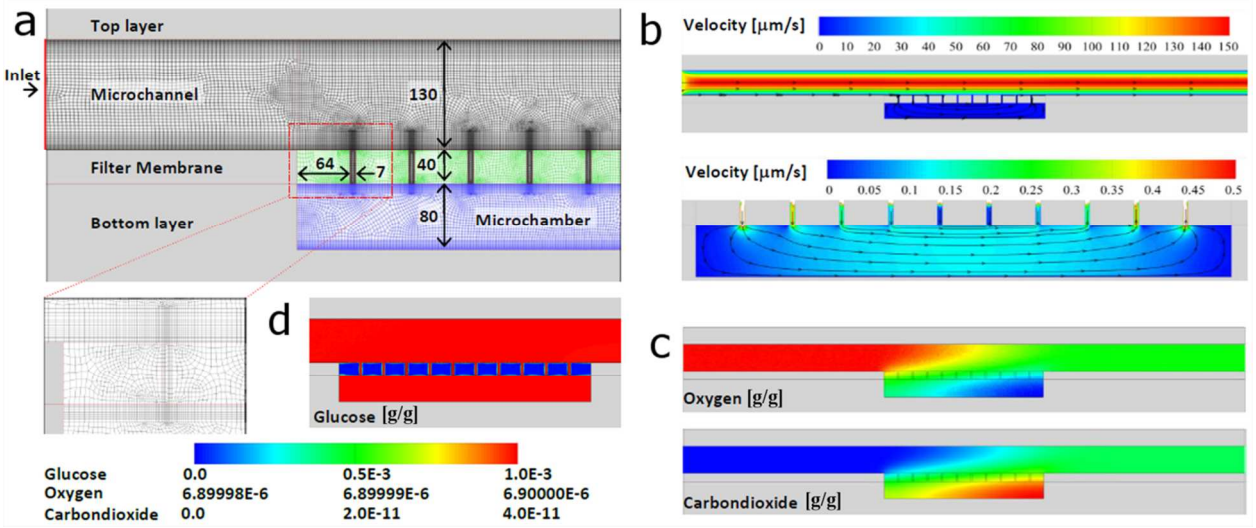

Figure 1. Computational fluid dynamics modeling (**a**) The geometry of the model (all dimensions are in μm), the microchannel and the microchamber details from the computational mesh. The mesh is formed by around 58,000 quadrilateral units with refinements near solid boundaries; (**b**) Velocity (μm/s) contours and streamlines in the entire device and in the chamber. Flow from left to right; (**c**) O_2 and CO_2 mass fraction (g/g) in the chamber; (**d**) $C_6H_{12}O_6$ mass fraction (g/g) in the entire device.

DISCUSSION

Respiration rate coefficients obtained from apples are not quite relevant to mammalian cell metabolism. We could not find any more relevant respiration data complete with details necessary to scale them to our case. Therefore, instead of generating results directly relevant to a particular cell type, in this study we aimed to 1) show the relevance of the transport mechanisms within the chamber of our device to those in interstitial flow, and 2) demonstrate our capability to simulate the transport as well as enzymatic reaction of species involved. We are working on measuring the glucose metabolic rate in cancer cell cultures, so that more relevant data will be used in our future simulations.

Variations in O_2 and CO_2 concentrations are actually negligibly small - we deliberately made them visible to show the details of simulation results. The legends of the contour plots show that mass fraction of O_2 is virtually constant and mass fraction of CO_2 is less than $4x10^{-11}$ (or $<4x10^{-5}$ ppm). Therefore the changes in O_2 and CO_2 concentrations are not expected to be enough to create any observable difference in metabolism of the cells at different locations in the chamber.

The transport within the chamber is diffusion-dominant: The Peclet number given by $Pe=LU/D$, where L is channel height (80 μm), U is average flow speed in the channel (~0.13 μm/s) and D is diffusion coefficient, is less than 0.015 for glucose and is even smaller for O_2 and CO_2. The pore structure of hydrogel results in a relatively low permeability region (i.e. high fluidic resistance) that largely hinders advective transport within the chamber. When the gel is removed in the simulations, the velocity magnitudes in the chamber become much larger. Therefore, a significant contribution to the fluidic resistance does come from hydrogel in the bottom microchambers as evidenced by an increased velocity after removing the gel during simulations (results not shown). The fluidic resistance created by the porous middle PDMS membrane is relatively insignificant as compared to that created by the gel.

References

(1) MH, M. *Standard Methods for the Examination of Water and Wastewater*, 12 ed.; American Public Health Association: New York, 1965.

(2) Daly, M. E.; Vale, C.; Walker, M.; Littlefield, A.; Alberti, K. G.; Mathers, J. C. *Am J Clin Nutr* **1998**, *67*, 1186-1196.

(3) Tarbell, J. M.; Shi, Z. D. *Biomech Model Mechanobiol* **2012**, *12*, 111-121.

(4) Wang, S.; Nagrath, D.; Chen, P. C.; Berthiaume, F.; Yarmush, M. L. *Tissue Eng Part A* **2008**, *14*, 227-236.

(5) Haynes, W. M. *CRC Handbook of Chemistry and Physics*, 93 ed.; NIST, 2007.

(6) Cussler, E. L. *Diffusion: Mass Transfer in Fluid Systems* 2ed.; Cambridge University Press: New York, 1997.

(7) Jones, J. P., Page, J., Plant, R. ; University of Minnasota: Minneapolis, 1980.

(8) Garrett, R. H., Grisham, C. M. *Biochemistry*; Brooks Cole, 1999.

(9) Mahajan, P. V., Goswami, T. K. *Journal of Agricultural Engineering Research* **2001**, *79*, 399-406.

(10) Song, Y. K., H. K. Yam, K. L. *Journal of the American Society for Horticultural Science* **1992**, *117*, 925-929.

(11) McLaughlin, C. P., O'Beirne, D. *Journal of Food Science* **1999**, *64*, 116-119.

(12) Nei, D., Uchino, T., Sakai, N., Tanaka, S., *Postharvest Biology and Technology* **2005**, *37*, 277-285.

(13) Heydari, A., Shayesteh, K., Eghbalifam, N., Bordbar, H., Falahatpisheh,12: 145–9. *International Journal of Agriculture and Biology 12: 145–9.* **2010**, *12*, 145-149.

(14) Grover, W. H., Bryana, A. K., Diez-Silvac, M., Suresh, S., Higgins, J. M., Manalisa, S. R. *Proceedings of National Academy of Sciences of the United States of America* **2011**, *108*, 10992-10996.

(15) Swartz, M. A.; Fleury, M. E. *Annu Rev Biomed Eng* **2007**, *9*, 229-256.